Direct Observation of the Dynamics of Semiflexible Polymers in Shear Flow

Markus Harasim,[1] Bernhard Wunderlich,[1] Orit Peleg,[2] Martin Kröger,[2] and Andreas R. Bausch[1,*]

[1]*Lehrstuhl für Biophysik (E27), Technische Universität München, D-85748 Garching, Germany*
[2]*Department of Materials, Polymer Physics, ETH Zurich, CH-8093 Zurich, Switzerland*

(Received 18 September 2012; published 5 March 2013)

The flow behavior of polymeric liquids can be traced back to the complex conformational dynamics of polymer molecules in shear flow, which poses a major challenge to theory and experiment alike due to the inherently large number of degrees of freedom. Here we directly determine the configurational dynamics of individual actin filaments with varying lengths in a well defined shear geometry by combining microscopy, microfluidics, and a semiautomated moving stage. This allows the identification of the microscopic mechanisms and the derivation of an analytical model for the dynamics of individual filaments based on the balance of drag, bending, and stochastic forces.

DOI: 10.1103/PhysRevLett.110.108302 PACS numbers: 47.57.Ng, 47.27.N−, 47.60.Dx

The configurational dynamics of single polymers is key to our understanding of all the flow behaviors observed for polymer solutions and their non-Newtonian rheological properties. The flow induced stresses acting on polymers result either in stretch coil transitions or tumbling events, and depend on the mechanical properties of the polymer. While stiff rods, such as several viruses, organic filaments, or carbon nanotubes only exhibit rotational or tumbling motion, omnipresent flexible polymers (e.g., synthetic polymers such as nylon, silicone or biological polymers like PEG and DNA) show all types of dynamics such as wriggling, breathing, and irregular tumbling motion [1–8]. These dynamics are the origin of the macroscopic viscous properties of polymeric liquids, such as drag reduction in turbulent flows or normal stresses causing rod climbing and Weissenberg effects, but they also dominate microscopic systems like lab on the chip applications, gene sequencing, or molecular electronics [9–12]. For semiflexible polymers a flow induced buckling has been described [13], which is one form of polymer dynamics leading to biological self-organization phenomena, such as cytoplasmic streaming effects or cilia synchronization [14]. Since the seminal papers of Chu, Shaqfeh *et al.* [15,16], where the behavior of single DNA filaments under simple extensional flow was first observed, intensive efforts have been made to describe the apparently complex polymer dynamics in detail. The filaments' response to flow was found to be determined by their entropic elasticity and it was possible to model their behavior via simulations or dumbbell models [5,17–20] and to study ensemble properties rather than the dynamics of individual flexible molecules by a mean field approach and normal mode analysis [3,21–24]. For flexible filaments, three modes of shear-induced stretching transitions had been discussed [25]: recoil, restretch, and tumble. Cross correlations between thickness and extension fluctuations revealed a causal relationship leading to four phases of motion: thickening, stretching, thinning, and crumpling recoiling. In the opposing limit of thermal [26] and nonthermal [27] rodlike filaments the polymer conformation is set by the bending energy.

An experimental confirmation as well as the continuous description, which captures the regime from stiff to truly semiflexible, is still lacking. To this end the origin and effect of the force balances acting on single polymers need to be identified. Yet, the experimental observations are limited by the optical resolution, which does not allow the resolution of the local configurational dynamics of *flexible* polymers.

Here we present the direct visualization of the tumbling dynamics of quite *stiff* and *semiflexible* linear polymers in shear flow and an analytical description of the observed dynamics. By combining microscopy, microfluidics, and a semiautomated moving stage we are in the position to directly determine the configurational dynamics of individual actin filaments with varying lengths in a well defined shear geometry. The observed dynamics is fully described by a telescopic Brownian rod model for the filament's end-to-end vector, where the ends of the telescope are confined to travel around a stadium track at a fixed arc distance. Although the shear flow strongly bends the filament during the tumbling, we find that the Brownian rod dynamics of stiff filaments holds for the end-to-end vector orientation of semiflexible filaments as well. The analytical model allows us to recover the spatial configurations during the tumbling motion as well as the average tumbling time without any fitting parameters.

Semiflexible actin filaments, polymerized by standard protocols (see the Supplemental Material [28]), exhibit tumbling motions, when put into a steady shear flow (rate $\dot{\gamma} \approx 4$–$20\ \mathrm{s}^{-1}$), which is realized here in a microfluidic device (the technical details of the experiment are described in the Supplemental Material [28]).

By following the flow of individual, nonextensible actin filaments, with different contour lengths L_c, by means of a motorized stage we are able to observe up to 40 tumbling events for individual filaments. During each tumbling event,

two distinct phases can be identified: a period of orientational alignment in the flow direction, governed by the rotational diffusion of the extended filament, and a rather deterministic period where advective transport results in the end-over-end tumbling of the polymer (see Fig. 1(a) and the movies in the Supplemental Material [28]).

The stochastic nature of the diffusive phase is directly visible in the varying duration between tumbling events [see Fig. 1(b)]. The deterministic nature of the advective phase is also evident from the regular shaped dips in the trajectory of the end-to-end distance R_{ee} [see the inset of Fig. 1(c)]. The total tumbling time needed for the end-to-end vector to flip its direction is clearly dominated by a phase, where it approaches a flow aligned state. Within the advective phase a characteristic U-turn-like configuration is typically achieved, which seems to exhibit a characteristic L_c-independent curvature radius of $\sim 1\ \mu$m [see Figs. 1(c) and 1(d)], consistent with the pronounced dip in R_{ee}/L_c from which the tumbling time is most conveniently determined.

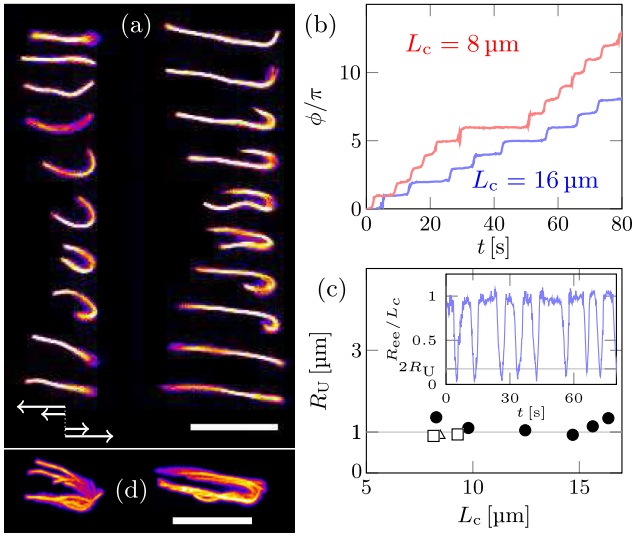

FIG. 1 (color online). (a) Successive images of two fluorescently labeled actin filaments of length 8 μm (left) and 16 μm (right) experiencing a mean shear rate of $\dot{\gamma} = 6\ \mathrm{s}^{-1}$. The fluid motion in the filaments' center of mass frame is sketched in the lower left corner (scale bar: 10 μm). (b) The time course of the orientational angle ϕ exhibits characteristic steps of π for every interchange of filament orientation. The steps are followed by extended plateaus around multiples of π of varying length which are identified with extended periods of flow alignment. (c) The mean curvature radius R_U of the filament's U-turn-like conformation does not change significantly for filaments of different contour lengths L_c. (filled circle $\dot{\gamma} \sim 6\ \mathrm{s}^{-1}$, open square $\dot{\gamma} \sim 12\ \mathrm{s}^{-1}$, open triangle $\dot{\gamma} \sim 19\ \mathrm{s}^{-1}$). (Inset) The end-to-end distance of a 16 μm filament shows alternating dips and plateaus, which reflect the stages of bending and full extension for every tumbling cycle. (d) Overlay of the conformations shown in (a). Both filaments follow a U-turn-like motion in which most of the filament segment remains flow aligned (scale bar: 10 μm). See the movies in the Supplemental Material [28].

We set out to demonstrate that the experimentally observed transient behavior of actin filaments can be rationalized by considering simple force balances for a model filament traveling through an ideal U-shaped turn. As the actin filaments are very thin compared to their length, exhibiting a diameter to length ratio $d/L_c \approx 10^{-3}$, a filament experiences virtually no torque in its fully extended, flow aligned conformation. A rotational, thermal fluctuation away from the aligned configuration brings the filament into a slightly tilted and eventually bent position, where both filament ends experience drag forces in opposing directions. The accompanying torque triggers a deterministic rotation of the filament. Fluctuations *against* the rotational direction of the shear flow are suppressed: the resulting drag forces induce an opposite rotation accompanied by a stretching of the filament which in turn drives the filament back into the aligned state. By contrast, fluctuations *along* the rotational direction of the shear flow are enhanced: the drag induces a rotation into the same direction, which is accompanied by a compressive force along the filament. The magnitude of the drag forces increases with increasing out-of-flow extension of the filament. Altogether, there exists a critical end-to-end orientation angle ϕ_c of the end-to-end vector, where the drag force is dominant over the thermal fluctuations, separating the advective and diffusive phases of the tumbling motion.

During the advective phase, above ϕ_c, the frictional forces may exceed the buckling force of the filament resulting in a U-turn like configuration with a radius R_U [see Fig. 1(d)], which can be readily computed by balancing the frictional forces with the elastic response of the filament (see the Supplemental Material [28])

$$R_U = \left(\frac{4}{\pi}\frac{k_B T L_p}{c_\parallel \dot{\gamma}}\right)^{1/4}, \tag{1}$$

where $\dot{\gamma}$ denotes the shear rate, L_p is the persistence length of the filament, $c_\parallel$ is the friction coefficient per unit length for fluid motion tangential to the filament, and $k_B T$ is the thermal energy. For the studied shear rates the radius can be calculated via Eq. (1) to be $R_U \sim 1\ \mu$m, using $L_p = 16\ \mu$m for actin, in good agreement with the experimentally observed values [see Fig. 1(c)]. As the conformation travels through an approximate U-turn shape and the shear rates are known, the time spent within the advective phase can be estimated. The frictional forces, computed by the torque balance (see the Supplemental Material [28]), directly depend on the track (or line) velocity along the U turn. This velocity we derive to be approximately constant throughout the U-turn-like motion ($v \approx \dot{\gamma} R_U$), in agreement with experimental observations (see the Supplemental Material [28]).

This important result paves the way to derive the complete dynamics of the telescopic rod—its orientational as well as extensional time-dependent behavior. To this end we begin by computing the angular velocity for the

end-to-end vector $\mathbf{R}_{ee}(t)$ of the filament in the advective phase. Using the track velocity v we obtain for the rate of change of its orientation angle ϕ (see the Supplemental Material [28])

$$\dot{\phi} = \dot{\gamma}\sin^2\phi, \tag{2}$$

which coincides with the rotational component of the velocity field of simple shear flow. It is important to realize that the rotational speed of the model actin filament is thus insensitive to its length. Equation (2) has a simple analytical solution and is supported by the experimentally determined angular velocities of the end-to-end vector shown in Fig. 2(a), as they do not depend on the contour length. Recalling that we find the filament's end-to-end vector to behave as a telescopic rod moving with both of its ends along an opposing U-shaped (stadium) conformational space with a known curvature radius R_U, we have an explicit prediction for the transient extension $R_{ee}(t)$ as well. Its time dependence basically results from geometric relationships between line distance and spatial distance on a stadium-shaped geometry (see the Supplemental Material [28]). For the length we obtain, for example, $R_{ee}(t) = 2R_U[1 + (\dot{\gamma}t)^2]^{1/2}$ ($R_U \ll L_c$) in the close vicinity of the sharp dips visible in the inset of Fig. 1(c). A quantitative analysis of the dips and the full telescopic dynamics for arbitrary L_c and R_U is readily performed (see the Supplemental Material [28] for details). Although Eq. (2) results from a balance of bending and frictional forces and is found to describe the motion of semiflexible polymers, it turns out to be equivalent to the

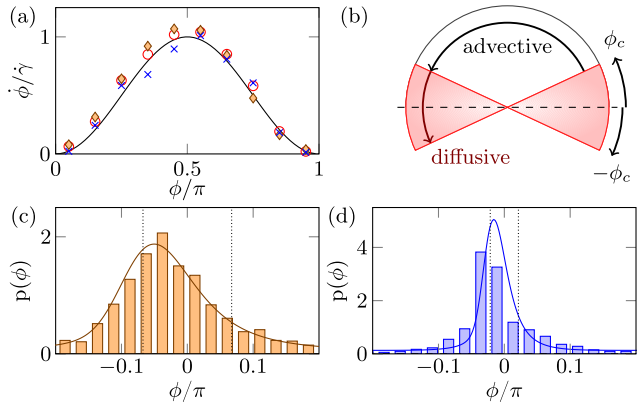

FIG. 2 (color online). (a) Angular velocity $\dot{\phi}$ vs orientation angle ϕ of actin filaments with lengths of 4 μm (diamonds), 8 μm (crosses), and 16 μm (open circles). All filaments show quite similar behavior, supporting our prediction, Eq. (2) (black line). (b) The orientation angle ϕ shows a predominantly deterministic motion during the advective phase, namely the passage between ϕ_c and $\pi - \phi_c$, followed by a diffusive phase between $\pi - \phi_c$ and $\pi + \phi_c$ where the realignment is superimposed by a rather diffusive motion. (c) and (d) Probability distributions of the orientational angle are shown for a quite stiff 4 μm actin (c) and 16 μm filament (d) at a shear rate $\dot{\gamma} \approx 4\,\mathrm{s}^{-1}$. The theoretical prediction for a rodlike polymer are overlayed as a solid line.

Jeffery equation [27], which describes the rotational velocity of a nonthermal rigid rod in the limit of thin rods. Thus the end-to-end vector of the strongly bent filament rotates during the advective U-turn phase equivalently to an infinitely thin rigid rod [see Fig. 2(a)], and the time spent in this phase, $\tau_{adv} = 2\dot{\gamma}^{-1}/\tan\phi_c$, follows directly from Eq. (2).

In the remaining diffusive phase, below ϕ_c, the filament is only weakly bent and behaves in a first approximation as a Brownian rod with a constant contour length L_c. During this phase the dynamics is set by the shear rate and the rotational diffusion coefficient of a rod $D_{rod} = 6k_BT/c_{\|}L_c^3$, which scales with L_c^{-3}, and can also be used to rewrite Eq. (1). For the time spent in the diffusive phase we obtain $\tau_{diff} \approx (5/3)\phi_c^2/D_{rod}$, as this time corresponds to the mean first passage time (see the Supplemental Material [28]) for ϕ to exceed ϕ_c, i.e., to leave the diffusive regime and to re-enter the advective phase.

Consequently, the complete tumbling dynamics of a semiflexible filament can be fully described by considering the motion of a telescopic Brownian rod in shear flow, where the orientational dynamics of the telescope coincides with the one for a Brownian rod of fixed length, and the extension dynamics is slaved to follow from the opposing U-shaped conformational space. In a Brownian rodlike tumbling motion, a deterministic advective phase with constant duration, in which the noise can be neglected, alternates with a thermally dominated phase around the flow aligned state at $\phi = 0$.

The transition between both regimes is given by the critical angle $\phi_c = (D_{rod}/\dot{\gamma})^{1/3}$ [see Fig. 2(b)] which has been obtained by equating the contributions of advection and diffusion to the stationary probability flux [29] of the angular motion. Evaluating the angular probability distribution function we see that the critical angle is indeed directly observable in our experiment and well described by the model of the Brownian rod, Figs. 2(c) and 2(d). The asymmetry of the experimentally observed angular distribution is due to the coupling of the flow gradient to the rotational diffusive behavior, which suppresses the fluctuations against the rotational direction of the shear flow. Considering $\phi_c^3 = 3\pi R_U^4/2L_c^3L_p \ll 1$ and recognizing that in this limit $\tau_{adv} = 2D_{rod}^{-1/3}\dot{\gamma}^{-2/3} = (6/5)\tau_{diff}$, we obtain for the total tumbling time of a semiflexible filament under strong flow conditions

$$\tau_T = \tau_{adv} + \tau_{diff} = \frac{11}{3}D_{rod}^{-1/3}\dot{\gamma}^{-2/3}, \tag{3}$$

where $D_{rod} \propto L_c^{-3}$ is insensitive to the flexibility of the filament. Interestingly, the obtained total tumbling time is independent of the exact nature of the U-turn-like motion. Thus the bending of the filaments should not affect the tumbling time. Indeed, the experiments confirm the notion that the semiflexible polymer dynamics is the same as expected for a stiff rod (see Fig. 3).

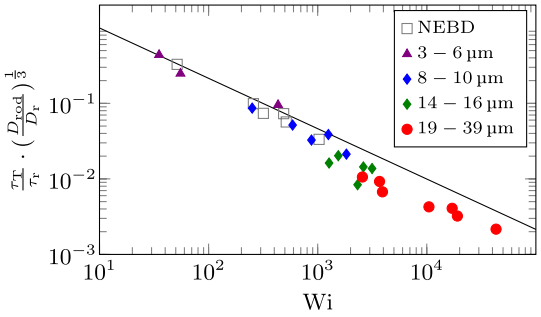

FIG. 3 (color online). Dimensionless tumbling times τ_T/τ_r multiplied by $(D_{rod}/D_r)^{1/3}$ of actin polymers at various shear rates plotted vs $\mathrm{Wi} = \dot{\gamma}\tau_r$. Contour length ranges are given in the legend. Tumbling times for the different shear rates decay as described by Eq. (4) (solid line); at strong flows a deviation can eventually be observed. Open squares show data points of nonequilibrium Brownian dynamics (NEBD) simulations for semiflexible polymers.

In our experiments we are also able to observe the dynamics of quite stiff rods, by considering filaments in the limit of short lengths (see Fig. 4). Indeed, filaments shorter than the computed buckling length $L_b = 2\pi^{3/4}R_U$ of $\sim 5\ \mu$m behave as predicted by the thermal stiff rod model (see Fig. 3). This is theoretically expected [4], yet experimental evidence was still lacking.

We can rewrite Eq. (3) introducing the Weissenberg number, $\mathrm{Wi} \equiv \tau_r\dot{\gamma}$, involving the orientational relaxation time τ_r of the semiflexible chain and the corresponding general rotary diffusion coefficient $D_r = 1/2\tau_r$ relevant for the dynamics of the end-to-end vector in equilibrium,

$$\frac{\tau_T}{\tau_r} = \frac{11 \times 2^{1/3}}{3}\left(\frac{D_r}{D_{rod}}\right)^{1/3}\mathrm{Wi}^{-2/3}. \qquad (4)$$

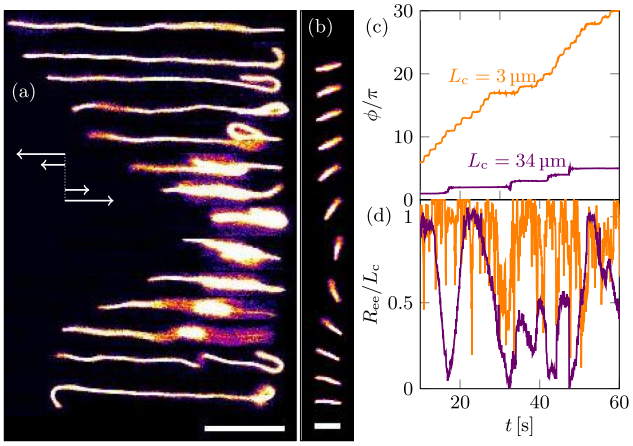

FIG. 4 (color online). Tumbling events of a (a) semiflexible 34 μm and (b) quite stiff 4 μm filament in steady shear with $\dot{\gamma} = 5\ \mathrm{s}^{-1}$. Multiple bending events occur during one tumbling event (see the Supplemental Material [28]). The fluid motion in the center of mass frame is sketched on the left [scale bar: 10 μm in (a) and 3 μm in (b)]. (c) Time course of orientational angle ϕ. (d) Time course of end-to-end-distance R_{ee}.

For a semiflexible chain, R_{ee}^{eq} is analytically known and $D_r = D_{rod}(L_c/R_{ee}^{eq})^2$ (see the Supplemental Material [28]); $R_{ee}^{eq} = L_c$ in the limit of quite stiff chains, by which Eq. (3) is recovered. By this the semiflexible regime and the stiff rod regime are fully described—without any fitting parameters.

In the limit of long filaments ($L_c \gg L_p$) the tumbling motion becomes more complicated, as the filament segments fluctuate independently, so that the filaments are able to exhibit two or more independent tumbling events simultaneously, where the turns can propagate separately with opposing directions through the filament. Such multiple tumblings can be induced at the ends of the filament as well as in their middle, and thus even loop formations can occur (see Fig. 4). This complex behavior illustrates that the complete change of the order of the end segments in flow can be reached in various ways. Yet, the advection of the polymer segments still obeys the Jeffery orbit. In this regime, where $\mathrm{Wi} > 2000$ the measured tumbling times decay slightly faster than expected from Eq. (4). Considering the buckling length of the filament, we compute the critical buckling Weissenberg number $\mathrm{Wi}_b \propto (L_c/2L_p)^{-3/2}$. For $\mathrm{Wi} < \mathrm{Wi}_b$ the stretching and compressing forces on the filament can be neglected during the diffusive phase. For $\mathrm{Wi} > \mathrm{Wi}_b$ buckling occurs already within the diffusive passage, so that the time τ_{diff} spent in the diffusive phase is shortened. Due to the strong compressive forces, $\mathrm{Wi} > \mathrm{Wi}_b$ is accompanied by multiple tumbling events, so that the dynamics is set by coupled segments of the filament which tumble individually. Thus, this regime could be equivalent with a regime found by simulations of flexible polymers to decay with $\propto \mathrm{Wi}^{-0.8}$ at high Peclet numbers (see Fig. 3) [19,20].

Until now all theoretical approaches relied on the comparison with the experimentally observed dynamics of DNA molecules under flow. Their persistence length of 50 nm, together with the used contour length of up to 80 μm results in rather complex configurational dynamics, where parts were not accessible by the optical resolution limit. Here the significantly increased persistence length of actin enables the direct optical accessibility of all dynamic processes, and the variation of the filament lengths enables the observation of a broad range of Weissenberg numbers spanning the quite stiff and the semiflexible regime.

The presented theoretical description in the framework of a rotating telescopic Brownian rod allows a unifying description for stiff and semiflexible linear polymers—based on the experimental observation and analytical derivation, that both the diffusive and advective phase obey the Jeffrey equation once extended to thermal rods. For flexible polymers, the contour length is significantly longer than the Kuhn length, and thus more complex dynamics is observed. However, under very strong flow conditions, the buckling length becomes shorter than the Kuhn length and the presented telescopic rod model will apply again for the motion of the individual Kuhn segments [19,20].

The identification of these microscopic mechanisms sets the basis for further developments of theoretical frameworks, which will aim for even more complex flow geometries and regimes above the overlap concentration, where the tumbling dynamics is expected to be the dominating mechanism resulting in unusual flow behavior. The introduced experimental approach may turn out to be instrumental to obtain microscopic evidence for these rather complex situations.

We thank M. Rusp for the actin preparation. This work was supported by Deutsche Forschungsgemeinschaft through Grant No. BA2029/8 and partly by the Cluster of Excellence Nanosystems Initiative Munich. M. H. and B. W. contributed equally to this work.

*Corresponding author.
abausch@ph.tum.de

[1] D. E. Smith, H. P. Babcock, and S. Chu, Science **283**, 1724 (1999).
[2] P. S. Doyle, B. Ladoux, and J. L. Viovy, Phys. Rev. Lett. **84**, 4769 (2000).
[3] J. S. Hur, E. S. G. Shaqfeh, and R. G. Larson, J. Rheol. **44**, 713 (2000).
[4] C. M. Schroeder, R. E. Teixeira, E. S. G. Shaqfeh, and S. Chu, Phys. Rev. Lett. **95**, 018301 (2005).
[5] S. Gerashchenko and V. Steinberg, Phys. Rev. Lett. **96**, 038304 (2006).
[6] J. S. Lee, E. S. G. Shaqfeh, and S. J. Muller, Phys. Rev. E **75**, 040802 (2007).
[7] R. Chelakkot, R. G. Winkler, and G. Gompper, Europhys. Lett. **91**, 14 001 (2010).
[8] D. Steinhauser, S. Köster, and T. Pfohl, ACS Macro Lett. **1**, 541 (2012).
[9] H. Craighead, Nature (London) **442**, 387 (2006).
[10] J. Sidorova, N. Li, D. Schwartz, A. Folch, and R. Monnat, Nat. Protoc. **4**, 849 (2009).
[11] G.-L. He, R. Messina, H. Löwen, A. Kiriy, V. Bocharova, and M. Stamm, Soft Matter **5**, 3014 (2009).
[12] G. Yu, A. Kushwaha, J. K. Lee, E. S. G. Shaqfeh, and Z. Bao, ACS Nano **5**, 275 (2011).
[13] V. Kantsler and R. E. Goldstein, Phys. Rev. Lett. **108**, 038103 (2012).
[14] T. Sanchez, D. Welch, D. Nicastro, and Z. Dogic, Science **333**, 456 (2011).
[15] D. E. Smith and S. Chu, Science **281**, 1335 (1998).
[16] C. M. Schroeder, H. P. Babcock, E. S. G. Shaqfeh, and S. Chu, Science **301**, 1515 (2003).
[17] M. Chertkov, I. Kolokolov, V. Lebedev, and K. Turitsyn, J. Fluid Mech. **531**, 251 (2005).
[18] A. Celani, A. Puliafito, and K. Turitsyn, Europhys. Lett. **70**, 464 (2005).
[19] I. S. Dalal, N. Hoda, and R. G. Larson, J. Rheol. **56**, 305 (2012).
[20] C. Sendner and R. R. Netz, Eur Phys J E Soft Matter **30**, 75 (2009).
[21] L. Harnau, R. G. Winkler, and P. Reineker, J. Chem. Phys. **104**, 6355 (1996).
[22] R. G. Winkler, Phys. Rev. Lett. **97**, 128301 (2006).
[23] R. G. Winkler, J. Chem. Phys. **133**, 164905 (2010).
[24] T. Munk, O. Hallatschek, C. H. Wiggins, and E. Frey, Phys. Rev. E **74**, 041911 (2006).
[25] R. E. Teixeira, A. K. Dambal, D. H. Richter, E. S. G. Shaqfeh, and S. Chu, Macromolecules **40**, 2461 (2007).
[26] J. K. G. Dhont and W. J. Briels, in *Soft Matter* (Wiley-VCH, Weinheim, Germany, 2007), pp. 147–216.
[27] G. B. Jeffery, Proc. R. Soc. A **102**, 161 (1922).
[28] See Supplemental Material at http://link.aps.org/supplemental/10.1103/PhysRevLett.110.108302 for theoretical derivations, experimental details and movies.
[29] H. Kobayashi and R. Yamamoto, Phys. Rev. E **81**, 041807 (2010).